Received: 13 June 2017 | Revised: 7 August 2017 | Accepted: 8 August 2017

DOI: 10.1002/aoc.4071

FULL PAPER

WILEY Applied Organometallic Chemistry

Ferrocene-substituted bis(ethynyl)anthracene compounds as anticancer agents

Ajeet Singh[1] | Pratibha Kumari[2] | Abhinav Raghuvanshi[1] | Shaikh M. Mobin[1,2,3] | Pradeep Mathur[1]

[1] Discipline of Chemistry, School of Basic Sciences, Indian Institute of Technology Indore, Simrol 453552, India

[2] Centre for Biosciences and Biomedical Engineering, Indian Institute of Technology Indore, Simrol 453552, India

[3] Discipline of Metallurgical Engineering and Materials Science, Indian Institute of Technology Indore, Simrol 453552, India

Correspondence
Shaikh M. Mobin and Pradeep Mathur, Discipline of Chemistry, School of Basic Sciences, Indian Institute of Technology Indore, Simrol – 453552, India.
Email: xray@iiti.ac.in; director@iiti.ac.in

Three compounds (**1**–**3**) were synthesized, where ethynylferrocene is substituted at different positions of anthracene and anthraquinone, and their biological properties were investigated. Compounds **1**–**3** were characterized using NMR and mass spectroscopies and confirmed by their single-crystal X-ray structure. They were also characterized from electronic and photophysical properties. All three crystal structures were optimized using density functional theory calculations. The presence of C–H···π interactions in **1**–**3** leads to the formation of two- and three-dimensional networks. The bioactivity of **1**–**3** was expressed by molecular docking with various cancerous proteins, which participated in progression of cancer. Compound **2** displayed the best interaction with cancer-related Aurora A protein in terms of both binding energy (−10.61 kcal mol^{-1}) as well as inhibition constant (16.74 nM). The molecular docking result also coincides with cytotoxicity on cancer cell lines (A375, HeLa) and DNA/protein binding affinity.

KEYWORDS
anti-proliferative effect, centrosymmetric, chemotherapeutic, cytotoxic, incubation

1 | INTRODUCTION

The varying structures and properties of ferrocene-based compounds in various biological systems drive the arduous search of scientists to perceive the unrevealed concepts of their functionality, these compounds displaying interesting cytotoxic,[1,2] antimalarial,[3–5] antifungal[6] and DNA-cleaving[7] activities. Furthermore, interactions of ferrocene-based compounds with proteins and DNA are the recent focus of research because of the potential for the development of new therapeutic products which can show anticancer property and transportation viability throughout a physiological system through protein binding.

Several ferrocene compounds have so far been examined and screened as important candidates for pharmaceutics.[7–12] From the anthracene point of view, azonafide belongs to a well-known class of drugs.[13] The idea was to combine both to get improved biological activity of the resulting compounds. Although there are a few reports revealing the crucial biological activity of ferrocene bonded to mono-aromatic ring compounds,[10–12] the role of ferrocene bonded to poly-aromatic systems like anthracene is not reported in the field of medicinal biochemistry. Detailed study of the interactions of ferrocene-based compounds against various serum albumins is needed to understand the metallic–pharmaceutical pharmacokinetics and structure–activity relationships since they bind to several compounds.[14] The nature of the interaction between various ferrocenyl compounds and proteins, which have been observed until now, is confined in nature and it requires more research for generalization.[13,15–17]

Herein we report the synthesis of 9,10-bisferrocenylethynylanthracene (**1**), 1,8-bisferrocenylethynylanthracene (**2**) and 2,6-bisferrocenylethynylanthraquinone (**3**) by C—C cross-coupling reaction, and their structural and spectroscopic characteristics and biological activities.

2 | RESULTS AND DISCUSSION

2.1 | Synthesis of compounds 1–3

The reaction of dibromoanthracene with ethynylferrocene in a 1:2 molar ratio in tetrahydrofuran (THF)–triethylamine (TEA) using $Pd(PPh_3)_4$ as a catalyst led to the formation of C—C cross-coupled products **1** and **2**. Compound **3** was prepared in a similar manner by replacing dibromoanthracene with diiodoanthraquinone in toluene (Scheme 1). Toluene was used instead of THF because of the poor solubility of diiodoanthraquinone in THF. Compound **1** was earlier synthesized by Chawdhury *et al.*[18] but the crystal structure was not analysed.[18] Compounds **1**, **2** and **3** were characterized using ^{1}H NMR and ^{13}C NMR spectroscopies and high-resolution mass spectrometry (HRMS) and authenticated by single-crystal X-ray diffraction.

The ^{1}H NMR (400 MHz, $CDCl_3$) spectra of all the compounds show corresponding peaks for ferrocene (characteristic signal near 4 ppm showing two singlets for C_5H_5 and C_5H_4) and anthracene (Figures S11–S13). The ^{13}C NMR (100.635 MHz, $CDCl_3$) spectra of **1** and **3** show the typical peak of ferrocene near 25.16 MHz whereas it is shifted in the case of **2** (94.2 ppm) which may be due to the one side distribution of electron density of ferrocene (Figures S14–S16). The infrared (IR) spectra of **1**–**3** show a noticeable band at *ca* 2200 cm^{-1} corresponds to $\nu_{C\equiv C}$ stretching mode. The band at 1672.05 cm^{-1} is $\nu_{C=O}$ stretching frequency observed for **3** as the characteristic peak of anthraquinone as compared to free anthraquinone (1675 cm^{-1}). There is not much effect of ferrocene electron density on $\nu_{C=O}$ stretching frequency. The out-of-plane C—H vibration B_{2u} modes are present at 1620.14, 1632.20 and 1591.35 cm^{-1} in **1**–**3**, respectively. At around 1575 cm^{-1}, there should be a band of $\nu_{C=C}$ stretching frequency but this band is overlapped by the out-of-plane vibrations in **1**–**3**. The out-of-plane C—H

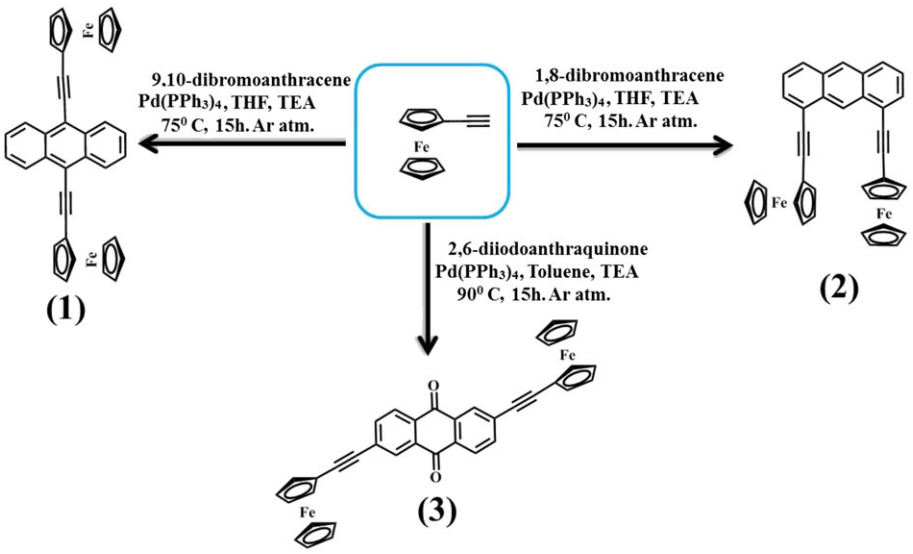

SCHEME 1 Synthesis of **1**–**3**

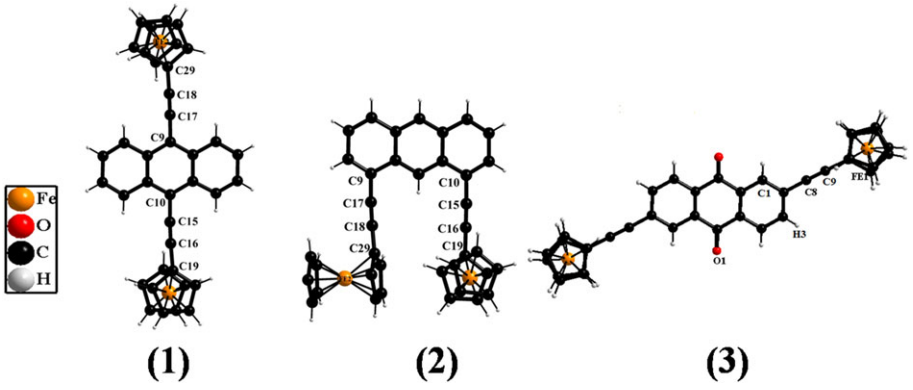

FIGURE 1 Perspective views of **1**, **2** and **3**

bending mode is observed in **1**–**3** at 1051.76, 1020.30 and 1035.59 cm^{-1}, respectively. The =C—H stretch peaks were at 3091.93, 3095.05 and 3103.71 cm^{-1} for **1**–**3**, respectively (Figures S17–S19). The HRMS spectra of **1**–**3** show the molecular ion peaks at 594.07, 594.08 and 624.1, respectively (Figures S20–S22). The structures of the compounds were also confirmed by single-crystal X-ray analysis.

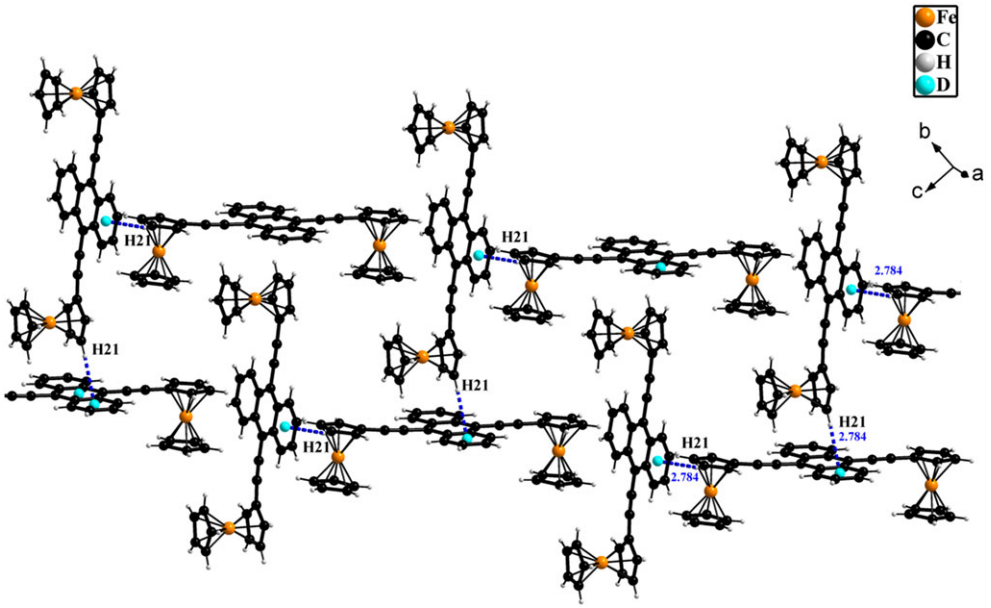

FIGURE 2 Two-dimensional network of **1** along tilted *a*-axis

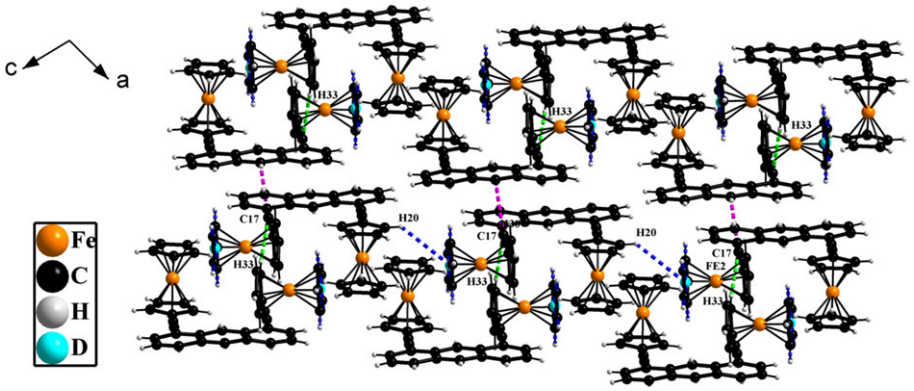

FIGURE 3 Three-dimensional network of **2** along *b*-axis

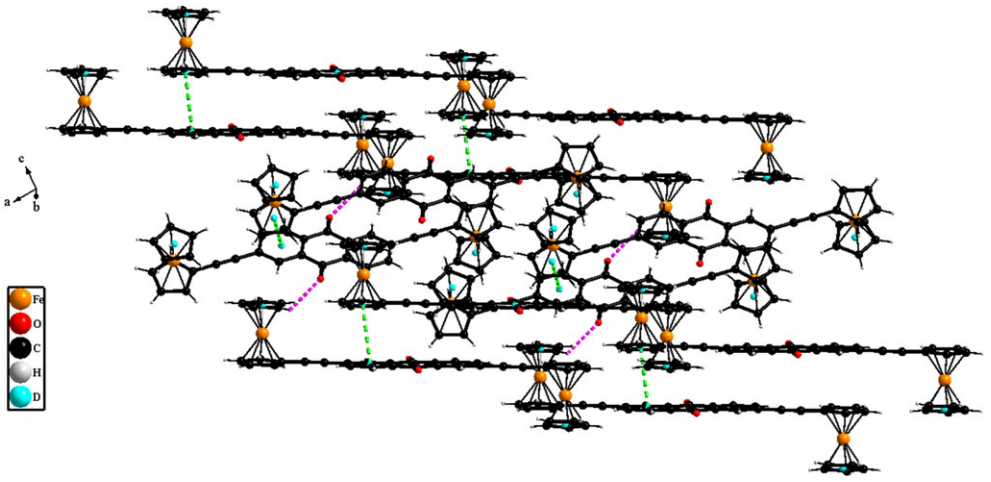

FIGURE 4 Three-dimensional network of **3** along tilted *b*-axis

2.2 | Molecular structures of 1–3

Compounds **1**–**3** crystallized in a centrosymmetric monoclinic system (Figure 1). The ferrocene units are found to be staggered in **1**–**3**. A small deviation from linearity was observed in **1**; the C10—C15—C16 angle is 177.09° and the C9—C17—C18 angle is 178.63°. Consequently, the —C≡C— bond deviates 2.91° and 1.57° out of the anthracene plane. Similarly, for **2** and **3**, the —C≡C— bond also slightly deviates from linearity. In **1**, the two ferrocenes are on the same side of the anthracene plane whereas, in **3**, they are on opposite sides. In the case of **2**, as the two ferrocenes are at 1- and 8-position, they align themselves perpendicular to each other to minimize steric crowding.

The packing diagrams of **1**–**3** show the presence of intermolecular C—H···π interaction which forms a one-dimensional polymeric chain (Figures S1, S2 and S4). Each one-dimensional polymeric chain is extended via C—H···π interactions between two adjoining layers, giving rise to the formation of a two-dimensional network (Figure 2, and Figures S3 and S5). Compounds **2** and **3** form three-dimensional networks using C—H···π and π···π interactions, respectively (Figures 3 and 4).

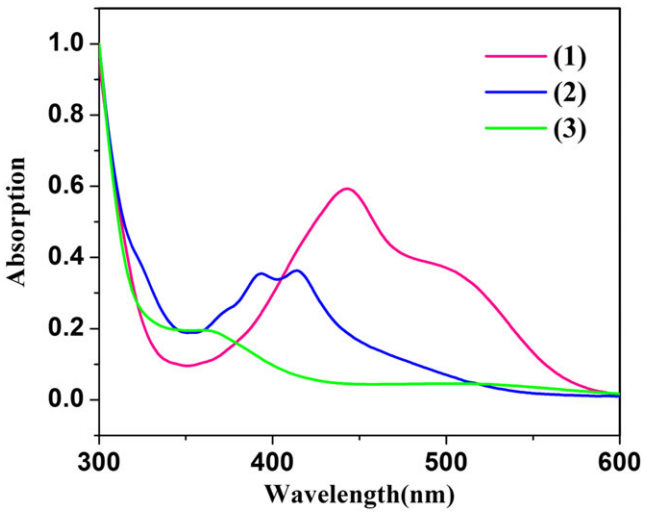

FIGURE 5 UV–visible spectra of **1**, **2** and **3**

2.3 | Electronic absorption spectra

The electronic absorption spectra of **1**–**3** were recorded in chloroform at room temperature (RT) (Figure 5 and Table S2). The absorption spectra show two dominating absorption peaks. That of **1** shows absorptions at 443 and 513 nm, that of **2** at 390 and 413 nm, and that of **3** at 360 and 515 nm, which correspond to the π–π* and metal-to-ligand charge transfer transitions.[19] Similar to our previously reported compounds,[20] the absorption maximum of 9,10-substituted anthracene compound **1** was found to be red-shifted, which suggests more perturbation of the 9,10-substituents on the anthracene ring.

2.4 | Density functional theory (DFT) calculations

In order to understand geometry optimization, energy and electronic communication in **1**–**3**, DFT calculations are carried out. The bond distances calculated for the optimized structures in **1**–**3** are similar to those obtained from their X-ray crystal structures. The frontier molecular orbitals of **1**–**3** are shown in Figure 6. For **1** and **2**, the highest occupied molecular orbitals (HOMOs) are of π-type and the lowest unoccupied molecular orbitals (LUMOs) are of π*-type, and both are delocalized on the anthracene unit. However, in **3**, the HOMO is localized

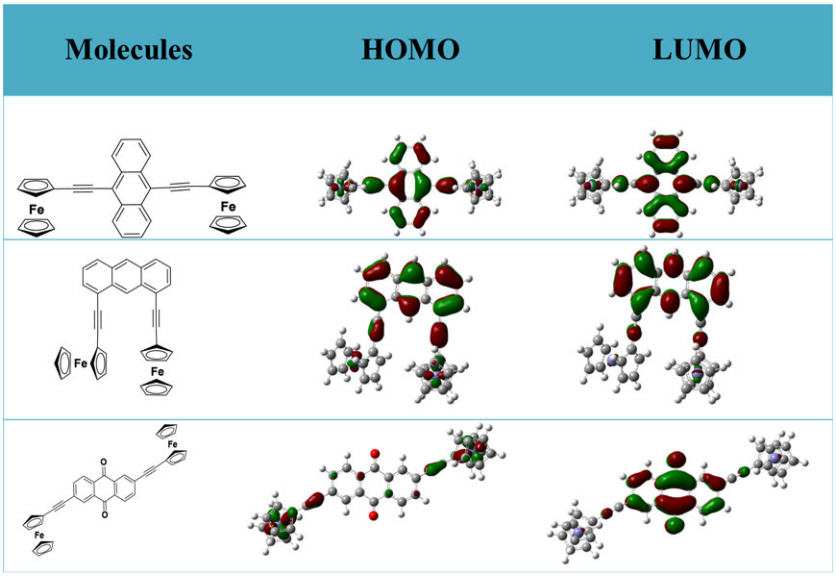

FIGURE 6 HOMO and LUMO of **1**, **2** and **3**

on the ferrocene unit, while the LUMO is on the anthraquinone unit. This reveals a particular donor–acceptor system, accompanied by the charge transfer process, where the ferrocenyl moiety behaves as donor and the anthraquinone part as acceptor.

2.5 | Molecular docking

To understand the binding affinity[21] and mode of interaction of proteins towards compounds **1**–**3**, molecular docking was done with three cancer-causing proteins. Based on parameters of inhibition constant, binding energy, van der Waals interactions and intermolecular energy between different proteins, several observations were made. Compound **2** strongly binds with cancer-related Aurora-A protein kinase (1MQ4)[22] with the interacting residues Gly140, Leu139, Lys141, Val147, Gly142, Ala160, Tyr212, Lys162, Ala213, Thr217, Gly216, Tyr219, Arg220, Leu263, Glu260, Asp274 (Figure 7, Table 1, Table S2) as compared to **1** and **3**.

In all cases, **1** and **2** are surrounded by both hydrophobic and charged amino acids of protein as shown in Figures S6 and S7 and Table 1. Compound **3** is mostly surrounded by hydrophobic and aromatic amino acids. Benzyl group of phenylalanine 181 and 406 is stabilized by cyclopentadienyl ring and anthraquinone of **3** by π···π stacking interaction (Figure S7). Inhibition constant of **2** towards cancer-related Aurora-A protein kinase is better than that of earlier reported compounds,[23] thus making **2** a potential candidate for further testing as an anticancer drug.

2.6 | Cell cytotoxic assay

The 3-(4,5-dimethylthiazole-2-yl)-2,5-diphenyltetrazolium bromide (MTT) assay can be used to determine the cell proliferation rate. When metabolic events lead to apoptosis or necrosis, MTT assay can be employed to measure the reduction in cell viability. The yellow tetrazolium MTT is reduced to purple-coloured formazan by metabolically active cells, by the action of dehydrogenase enzymes.[24] Here, this assay was used to examine the anti-proliferative effect[25] of **1**–**3** on human melanoma cancer (A375), cervical carcinoma (HeLa) and normal human embryonic kidney (HEK) cell lines. The cytotoxicity of **1**–**3** is found to be concentration dependent, i.e. average cell viability ratio decreases on increasing the concentrations of the compounds. The IC_{50} values for **1**–**3** after to 24 h of treatment are found to be 20.3, 15.1 and 25 μM, respectively, on A375 cells; 30.1, 25 and 35.2 μM, respectively, on HeLa cells; and >80 ± 0.013, 80 ± 0.099 and >120 ± 0.063 μM, respectively, on HEK cells (Figure 8 and Table 2). This suggests that the compounds are less toxic to the normal cell line as compared to cancerous cell lines. The *in vitro* cytotoxicity assay confirms that **2** exhibits higher cytotoxicity to the tumour cell lines and it may act as a potential chemotherapeutic agent against cancer.

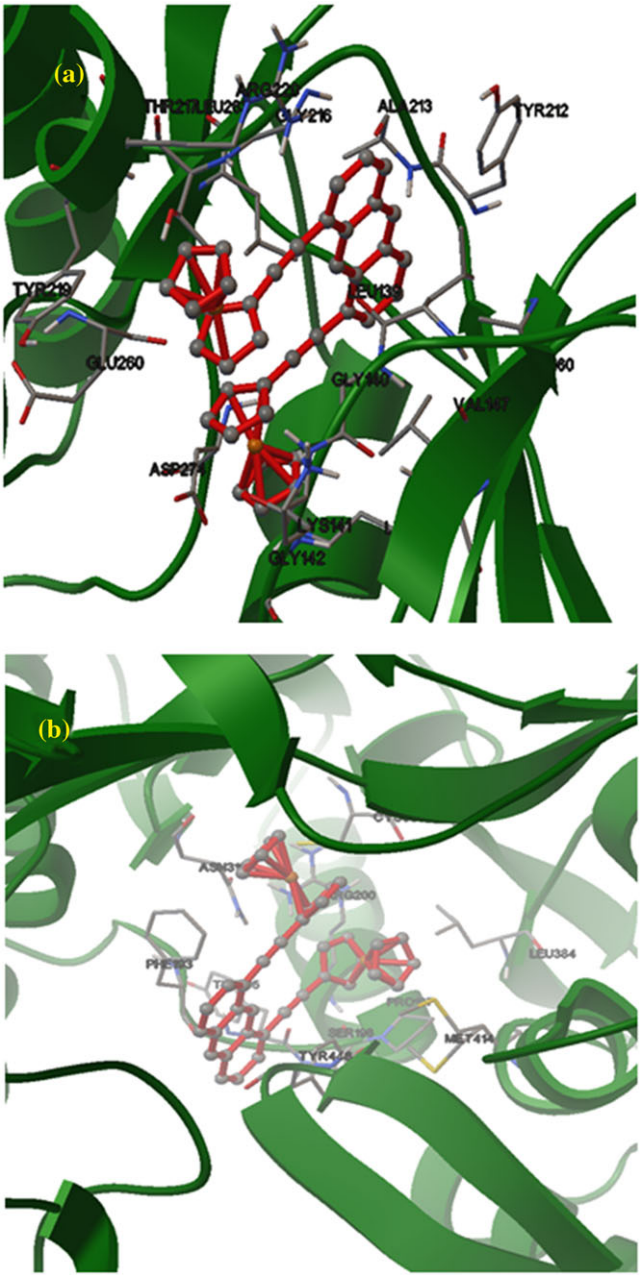

FIGURE 7 Molecular docking of **2** with cancer-causing and viral proliferation proteins. The proteins are shown as ribbons and the interacting residues are shown as sticks. The ligand is shown as ball and stick. (A) Cancer-related aurora-a protein kinase (1MQ4); (B) hepatitis C virus NS5B polymerase (2WCX)

2.7 | Bovine serum albumin (BSA) binding studies

The plasma proteins present in blood are necessary for transportation of drugs throughout the body. If molecules

TABLE 1 Molecular docking of **1**–**3** with cancer-causing proteins

Ligand	Protein (PDB ID)	Binding energy (kcal mol^{-1})	Inhibition constant	Interacting residues
1	Cancer-related aurora-A protein kinase (1MQ4)	−8.83	338.17 nM	GLY142, LYS143, PHE144, VAL147, LYS162, LEU164, GLN177, LEU210, LYS258, ASN261, LEU263, ALA273, ASP274, TRP277, CYS290
	Cancer-associated protein kinases ephrin A2 (ephA2) receptor protein kinase (1MQB)	−7.81	1.88 μM	ILE619, ALA621, GLY622, GLU623, PHE624, GLU663, TYR694, GLU696, ASN697, GLY698, ASP757, GLY759
	Cancer-related (FAK) focal adhesion kinase (1MP8)	−7.19	5.32 μM	ILE420, GLY429, GLY431, GLN432, PHE433, VAL436, ALA452, LYS454, GLU471, ASN551, LEU553, ASP564
2	Cancer-related aurora-A protein kinase (1MQ4)	−10.61	16.74 nM	LEU139, GLY140, LYS141, GLY142, VAL147, ALA160, LYS162, TYR212, ALA213, GLY216, THR217, TYR219, ARG220, GLU260, LEU263, ASP274
	Cancer-associated protein kinases ephrin A2 (ephA2) receptor protein kinase (1MQB)	−8.6	424.47 nM	ILE619, GLY620, ALA621, ALA644, LYS646, THR692, GLU693, TYR694, MET695, ALA699, ARG743, ASN744, LEU746, SER756, ASP757
	Cancer-related (FAK) focal adhesion kinase (1MP8)	−7.9	1.63 μM	ILE428, GLU430, GLY431, GLN432, ALA452, ILE454, GLU471, VAL484, MET499, GLU506, ARG550, ASP564
3	Cancer-related aurora-A protein kinase (1MQ4)	−9.01	250.47 nM	LEU139, LYS143, VAL147, LYS162, VAL174, GLN177, ALA213, GLY216, THR217, GLU260, ASN261, LEU263, ASP274, TRP277, THR288, LEU289, CYS290
	Cancer-associated protein kinases ephrin A2 (ephA2) receptor protein kinase (1MQB)	−7.94	1.52 μM	THR21, LYS23, HIS45, CYS45, PRO47, GLN56, PHE61, LYS112, LYS115, GLU116, ASN119
	Cancer-related (FAK) focal adhesion kinase (1MP8)	−7.24	4.9 μM	ILE428, GLY431, GLN432, ALA452, LYS454, GLN470, GLU471, LEU501, CYS502, GLY505, GLU506, ASP564

bind to them, the transportation of the drug will be affected. The interaction of organometallic compounds with proteins is generally examined in terms of the intrinsic fluorescence intensity. The interaction of compounds with BSA has been well studied by fluorescence quenching. The three amino acids that are responsible for the fluorescence property in BSA are tryptophan, tyrosine and phenylalanine residues. The quenching may happen for various reasons, such as the formation of ground-state complex, excited state reactions, molecular rearrangement, energy transfer and collision.[26]

To overcome the inner filter effect, we diluted the sample from 5 to 1 μM. When we plotted the normalization graph, we found there is no shift in wavelength of maxima (Figure S23). This suggests that at such concentration, we did not observe the inner filter effect. The spectra of **1**, **2** and **3** bound to BSA clearly show a marked decrease in the intensity of the fluorescence accompanied by a noticeable blue shift at 340 nm. The blue shift indicates that, after the addition of the compounds, the polarity around the fluorescence chromophore (such as tryptophan, tyrosine) of BSA decreases due to which the hydrophobicity increases and the peptide strands become less extended. The result suggests that the conformation of the protein slightly changes.[27,28] At 340 nm, the intensity of the fluorescence spectral band is quenched up to 40% of its initial value (Figure 9).

The maximum wavelength of emission is shifted to higher energy which shows the transfer of energy from the indole moiety present in tryptophan towards **1**–**3** attached to the specific protein. The fluorescence quenching data were understood in terms of the Stern–Volmer equation[29] (supporting information). The Stern–Volmer quenching rate constant (K_{SV}) values obtained are 1.00×10^3 M^{-1} for **1**, 1.19×10^4 M^{-1} for **2** and 1.00×10^4 M^{-1} for **3** (Table 3) which indicate a firm binding between **1**, **2** and **3** and BSA (Figure 9). The value of bimolecular quenching rate constant (K_q) of **1**, **2** and **3** is found to be 1×10^{11}, 1.19×10^{12} and 1×10^{12} M^{-1} s^{-1}, respectively (Table 3), indicative of static quenching. The varying concentrations of **1**, **2** and **3** show linearity in Stern–Volmer plots. This shows one stable ground-state complex formation in the BSA–**1**, BSA–**2** and BSA–**3** systems.[30]

To determine the number of binding sites and value of binding constant, the Scatchard equation is used (supporting information). The result obtained is a higher binding constant (5.6×10^6 M^{-1}) and n value (1.37) for **2**–BSA as compared to **1**–BSA (4.01×10^6 M^{-1}, 1.05) and **3**–BSA (4.8×10^6 M^{-1}, 1.19). These are also comparatively high values in comparison with many compounds

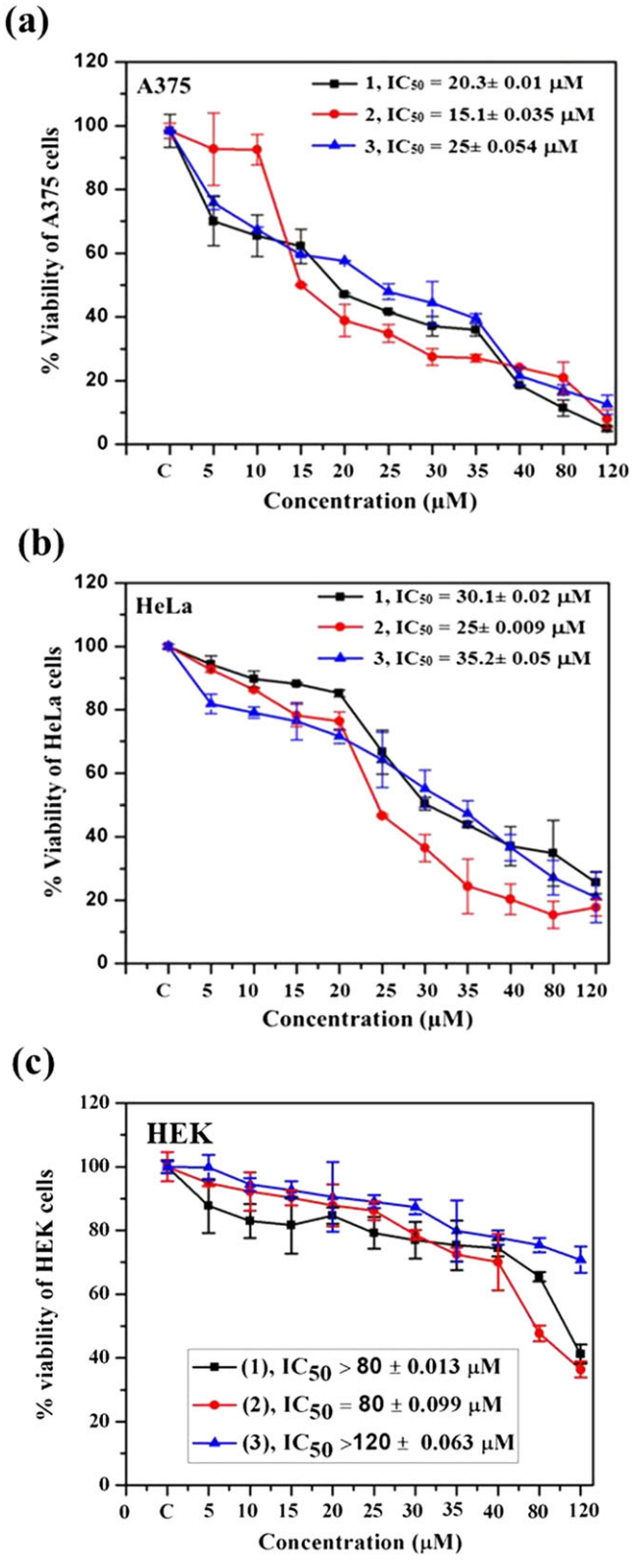

FIGURE 8 Cell viability studies of **1**, **2** and **3** on cancerous as well as normal cell lines. (a) HeLa cell line; (b) A375 cell line; (c) HEK cell line. These cells were exposed to various concentrations of **1**, **2** and **3** for 24 h and then cell viability was measured by MTT assay

TABLE 2 IC_{50} values (μM; mean (±SD), $n = 3$) evaluated from MTT assay for A375, HeLa and HEK cells treated with **1**, **2** and **3** for 24 h

Compound	A375	HeLa	HEK
1	20.3 ± 0.01	30.1 ± 0.02	>80 ± 0.013
2	15.1 ± 0.035	25 ± 0.009	80 ± 0.099
3	25.0 ± 0.054	35.2 ± 0.05	>120 ± 0.063

reported so far[31–33] (Table 3). A possible justification for the higher values is that **2** is more electron-releasing in nature than **1** and **3** due to its exposed orientation and the presence of electron-donating *cis*-ferrocenyl group; the comparatively higher electron density on anthracene ring may lead to greater interaction with the electron-withdrawing domain of the protein.

Moreover, molecular docking of **1**–**3** with BSA was also investigated. The result shows that **2** strongly binds with BSA as compared to **1** and **3** in terms of binding energy and inhibition constant, i.e. −9.29 kcal mol^{-1} and 154.9 nM, respectively. The residues interacting with **2** are Ser109, Pro110, Asp111, Arg144, His145, Pro146, Ala193, Arg196, Glu424, Ser428, Arg458. Hydrophobic amino acids like proline, tryptophan, leucine and isoleucine interact with **1**–**3** as depicted in Figure S25 and Table S4.

2.8 | DNA binding studies

DNA is considered as a vital target to mediate necrosis or apoptosis of cells. Therefore, the interactions of calf thymus DNA (CT-DNA) and **1**, **2** and **3** are investigated using UV–visible titration experiments. The binding to DNA leads to changes in the UV–visible spectra of complexes. This may be due to the change in the DNA conformation after binding with **1**–**3**. Hypochromism with negligible shift at 254 nm is observed, upon addition of **1**. But in the case of **2** and **3**, hypochromism with a blue shift at absorption maxima is observed at 258 and 254 nm, respectively. The hyperchromic effect with blue shift suggests that **1**–**3** bind to DNA by partial intercalation, external contact or may be due to electrostatic binding.[34] The intrinsic binding constants K_b are found to be 1.216×10^3, 3.51×10^3 and 5.27×10^2 M^{-1}, respectively, for **1**–**3**. From the binding constant values, it is inferred that **2** binds more strongly with CT-DNA as compared to **1** and **3** as shown in Figure S24.

The interaction of CT-DNA with compounds **1**, **2** and **3** can be understood by steady-state competitive binding experiments employing **1**–**3** as the quenchers. Ethidium bromide (EB) was used the fluorescent probe. EB emits intense fluorescence upon interaction with DNA because of intercalation of EB between

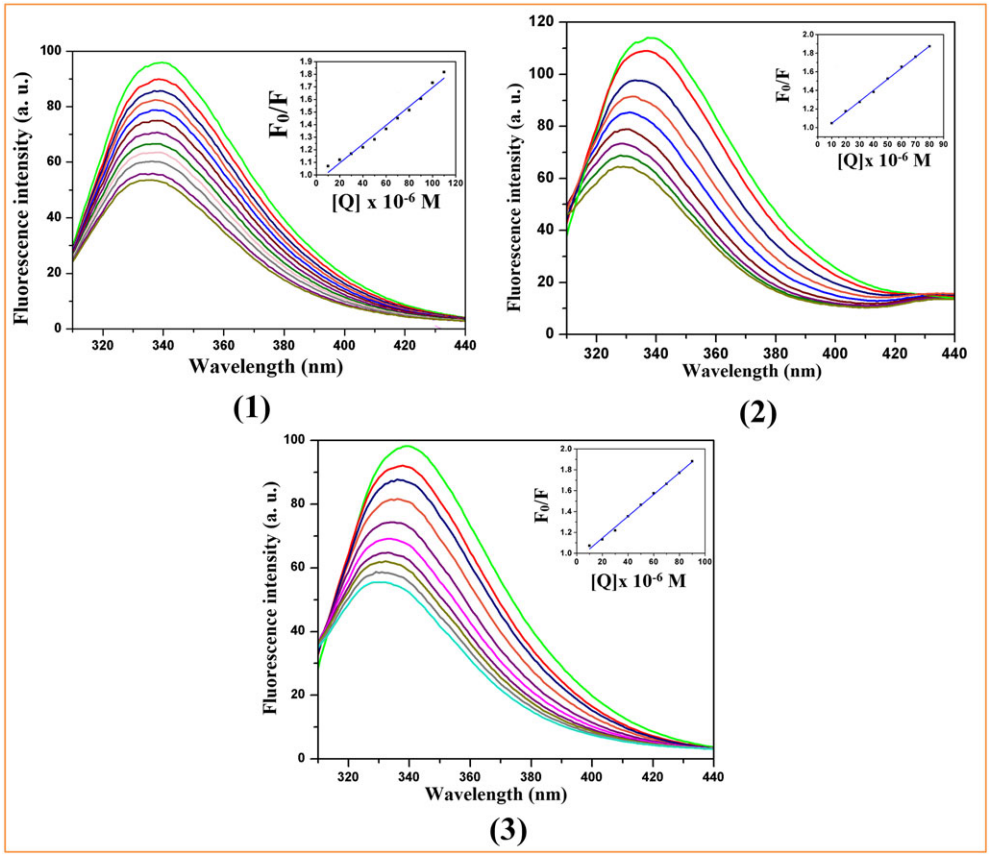

FIGURE 9 BSA binding of **1**, **2** and **3**. Insets: Corresponding stern–Volmer plots

DNA base pairs. When **1–3** intercalate into DNA, the binding sites in DNA for EB decrease, and therefore quenching of the fluorescence intensity is observed. This fluorescence intensity reduction reveals that **1–3** displace the EB molecules from the binding sites of DNA (Figure S9).

The phenomenon is more clearly visible for **2** as compared to **1** and **3**. Furthermore, K_q values for **1–3** are 5.6×10^3, 6.0×10^3 and 5.6×10^3 M^{-1}, respectively, which are obtained from the classical Stern–Volmer equation.[35] The binding constant (K_b) of **1**, **2** and **3** with CT-DNA obtained from double-logarithm equation $\log[(F_0 - F)/F]$ versus $\log[Q]$ is 3.34×10^6, 3.72×10^6 and 4.62×10^6 M^{-1}, respectively, reflecting favourable binding of **3** and DNA after displacing EB molecules attached to the DNA as compared to **1** and **2** (Figure S10).

TABLE 3 Stern–Volmer quenching constant, binding constant and number of binding sites with BSA

Compound	K_{SV} (M^{-1})	K_q (M^{-1} s^{-1})	K_b (M^{-1})	n
1	1.00×10^3	1.0×10^{11}	4.01×10^6	1.05
2	1.19×10^4	1.19×10^{12}	5.6×10^6	1.37
3	1.00×10^4	1.0×10^{12}	4.8×10^6	1.19

2.9 | Circular Dichroism (CD) studies

Conformational changes in protein helix perturbation in BSA upon interaction with **1**, **2** and **3** are noticeable from CD spectroscopic results. In the BSA CD spectrum, there are two major characteristic bands at 208 nm (negative) and 222 nm (negative) indicating a negative Cotton effect because of the n → π* transition in the peptide linkage of the α-helical structure (Figure 10). The conformational changes of the protein can be traced by the changes in the intensity and position of these spectral bands in CD spectra. Upon the interaction of **1**, **2** and **3** with BSA, these bands show an appreciable increase in intensity, which indicates that BSA binds to **1**, **2** and **3** and alters its native conformation.[36]

All these bands are observed to show an increase in intensity with addition of **1**, **2** and **3**, which can be assigned to the local perturbation of the native conformation of BSA α- and β-helix. The reason envisaged is that the hydrophobic domains in the protein chain have a hydrophobic interaction with the compounds. The perturbed amino acids of the protein assume a confirmation that facilitates its binding to **1–3**. The perturbation in α and β form of BSA is shown in Table S3. Interestingly **1** binding with BSA as a β-form is not seen at lower concentration. The composition of the

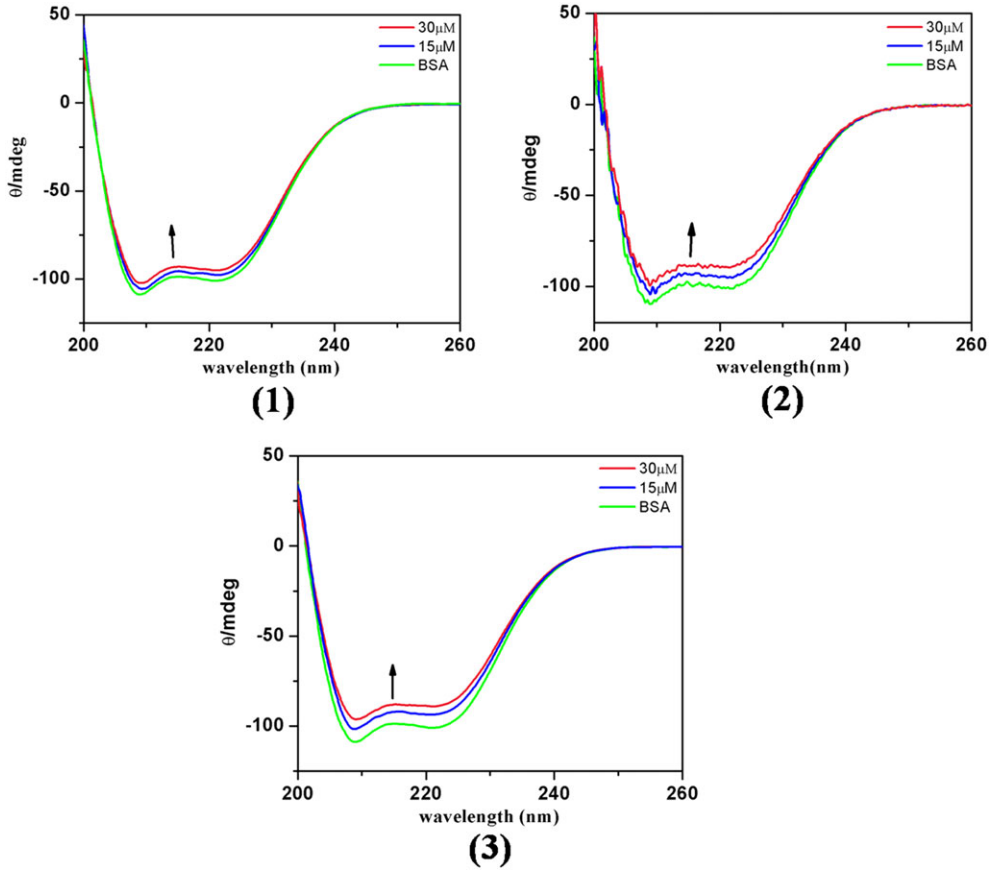

FIGURE 10 CD studies of **1**, **2** and **3**

TABLE 4 Crystal data and structure refinement for **1–3**

	1	2	3
Empirical formula	$C_{38}H_{26}Fe_2$	$C_{76}H_{52}Fe_4$	$C_{38}H_{24}Fe_2O_2$
Formula weight	594.29	1188.57	624.27
Temperature (K)	293 (2)	293 (2)	300.0
Crystal system	Monoclinic	Monoclinic	Monoclinic
Space group	$P2_1/c$	$P2_1/n$	$P2_1/n$
a (Å)	11.1693 (5)	15.0626 (5)	6.7940 (3)
b (Å)	17.3199 (6)	11.3239 (4)	18.4075 (9)
c (Å)	14.4292 (6)	16.9711 (7)	10.8529 (8)
α (°)	90	90	90
β (°)	96.725 (5)	104.276 (4)	99.160 (5)
γ (°)	90	90	90
Volume (Å^3)	2772.2 (2)	2805.32 (18)	1339.96 (13)
Z	4	2	2
ρ_{calc} (g cm^{-3})	1.424	1.407	1.547
μ (mm^{-1})	1.073	1.060	1.119
F(000)	1224.0	1224.0	640.0
Crystal size (mm^3)	0.23 × 0.18 × 0.13	0.330 × 0.220 × 0.180	0.32 × 0.27 × 0.23

(Continues)

TABLE 4 (Continued)

	1	2	3
Radiation	Mo Kα ($\lambda = 0.71073$)	Mo Kα ($\lambda = 0.71073$)	Mo Kα ($\lambda = 0.71073$)
2θ range for data collection (°)	5.968 to 49.994	6.122 to 64.338	5.836 to 49.994
Index ranges	$-13 \le h \le 13$, $-20 \le k \le 20$, $-17 \le l \le 17$	$-21 \le h \le 19$, $-16 \le k \le 11$, $-24 \le l \le 25$	$-7 \le h \le 8$, $-21 \le k \le 21$, $-12 \le l \le 12$
Reflections collected	21 315	38 077	10 009
Independent reflections	4878 [$R_{int} = 0.0760$, $R_{sigma} = 0.0587$]	9338 [$R_{int} = 0.0327$, $R_{sigma} = 0.0249$]	2351 [$R_{int} = 0.0291$, $R_{sigma} = 0.0205$]
Data/restraints/parameters	4878/0/362	9338/0/362	2351/0/190
Goodness-of-fit on F^2	1.118	1.039	1.099
Final R indexes [$I \ge 2\sigma(I)$]	$R_1 = 0.0803$, $wR_2 = 0.2080$	$R_1 = 0.0446$, $wR_2 = 0.1162$	$R_1 = 0.0420$, $wR_2 = 0.1110$
Final R indexes [all data]	$R_1 = 0.1256$, $wR_2 = 0.2587$	$R_1 = 0.0607$, $wR_2 = 0.1279$	$R_1 = 0.0485$, $wR_2 = 0.1176$
Largest diff. Peak/hole (e Å^{-3})	1.18/−1.00	0.53/−0.40	0.46/−0.20
CCDC no.	1503798	1503799	1503800

peptide's secondary structure is approximated by the CD spectra analysis from previous work.[37]

3 | CONCLUSIONS

We have synthesized two bisferrocenylethynylanthracene compounds (**1** and **2**) and a 2,6-bisferrocenylethynylanthraquinone compound (**3**) with substitutions at different positions of anthracene and anthraquinone rings. The results of biological activities of the compounds confirmed that **2** has more effective anticancer activity compared to **1** and **3** from both molecular docking and cell cytotoxic assay studies. Cytotoxic activities further confirm the binding of the compounds to DNA, which consequently leads to cell death.

4 | EXPERIMENTAL

All experiments were done under an inert atmosphere. All reaction solvents were distilled prior to use; freshly dried THF and TEA were used. Column chromatography was carried out using silica gel (230–400 mesh) as specified. All reagents were purchased either from Rankem or Sigma-Aldrich and used without further purification. NMR spectra were recorded in deuterated chloroform ($CDCl_3$) with a Bruker Avance (III) instrument. IR spectra were recorded with a Bio-Rad FTS 3000 MX instrument using KBr pellets. Mass spectra were recorded with a Bruker-Daltonics microTOF-QII mass spectrometer. All UV data were measured at RT at a concentration of 10^{-4} M in chloroform with a Varian UV–visible spectrophotometer (Cary 100).

4.1 | X-ray crystallography

Data were collected at 293 K using graphite-monochromated Mo Kα ($\lambda_\alpha = 0.71073$ Å). The data collection strategy was interpreted by employing CrysAlisPro CCD software. The collection of data was done by the standard phi–omega scan techniques. The data were scaled and reduced employing CrysAlisPro RED. The direct method using SHELXS-97 was used to solve the crystal structures and refined by the full matrix least squares method with SHELXL-97, refining on F^2.[38] The hydrogen atoms were placed at geometrically constrained positions and refined using isotropic temperature factors, generally $1.2 \times U_{eq}$ of their parent atoms. All remaining non-hydrogen atoms were refined anisotropically. All the C—H···π interactions, molecular drawings and mean plane analyses were obtained using Diamond (version 3.1d) and Mercury (version 3.1). The crystals and their refinement data are summarized in Table 4 and selected bond angles and bond distances in Table S1.

4.2 | DFT calculations

In order to explore the electronic structure and optimize the structure of **1**–**3**, DFT calculations were performed using the Gaussian09 program.[39] All calculations were

done at the B3LYP[40,41] level of theory employing the Lanl2DZ basis set for Fe and 6-31G* basis set for the remaining atoms. The geometries were optimized without imposing symmetry or any other restraints.

4.3 | Molecular docking

On the basis of a literature survey, the structural data of three different proteins were downloaded from the Protein Data Bank. The examined proteins were cancer-related Aurora-A protein kinase, ephrin A2 (ephA2) receptor protein kinase (cancer-associated protein kinases), cancer-related focal adhesion kinase (FAK) and bovine serum albumin (4F5S).

AutoDock 4.2[42] employing the Lamarckian genetic algorithm was used for the docking of ligands with proteins. The coordinates of **1**–**3** were utilized from crystal structures as a .cif file and saved as the. PDB format using Mercury software. The water molecules and co-crystallized inhibitors were omitted from all the protein structures. Polar hydrogen atoms and Gastegier and Kollman charges were given. All other bonds had rotational freedom. MGL AutoDock Tool was used to generate the grid parameter file of each protein. A grid-box was made to cover the entire protein domain. The centre of the protein structure was considered as the centre of the grid-box. The value of 0.375 was used as the spacing between grid points for all protein structures. After finalization of grid map, AutoDock was run. The population size of the genetic algorithm was 150 and the maximum number of energy evaluations and generations were 2 500 000 and 27 000, respectively. A maximum number of top individuals that survived automatically was set to 1 having mutation and crossover rates of 0.02 and 0.8, respectively. The parameters were the same for all target proteins. The docking calculation resulted in 10 different conformations. The best conformation was selected based on the lowest binding energy and inhibitory constant.

4.4 | MTT assay

The MTT assay was performed to examine the effect of **1**–**3** on cell viability. A375, HeLa and HEK cell lines were used in our study. Minimum essential medium (Himedia) supplemented with 10% foetal bovine serum and 1% antibiotics penicillin/streptomycin, 10 000 U ml^{-1}, was used for the culture of both A375 and HeLa cells. Dulbecco's modified Eagle medium was used for the culture of HEK cells. To perform cell viability assay, 8000 cells per well in 100 μl of complete media were seeded in triplicates into 96-well plates and cell adhesion was done after incubation for 24 h in 5% CO_2 atmosphere at 37 °C. After cell adhesion, **1**–**3** were completely dissolved in 0.1% dimethylsulfoxide (DMSO) at different concentrations and 10 μl of the solution was added to each well to give a final concentration with the range 5–120 μM. DMSO (0.1%) was added as the control. Cell viability assay was assessed using standard MTT assay.[43] After 24 h of incubation, 100 μl of MTT (0.5 mg ml^{-1}) was added to each well and incubated for another 4 h. The medium was then removed and 100 μl of DMSO was added and was shaken for 10 min in order to dissolve formazan crystals. Absorbance at a wavelength of 570 nm was measured with a Synergy H1 Biotek microplate reader. The cell viability data were calculated as % cell viability = [mean OD of treated cells (control)/mean OD of untreated cells (control)] × 100. IC_{50} (half maximal inhibitory concentration) values were obtained using the relative viability over **1**–**3** concentration graph.

4.5 | DNA binding studies

CT-DNA binding studies were performed by UV–visible and fluorescence spectroscopic methods. In UV–visible titration experiments, compounds were dissolved in 50 μM Tris–HCl buffer in THF (7:3, *v*/v). The concentration of CT-DNA was determined by measuring absorption intensity at 260 nm employing ε_{260} of DNA as 6600 $dm^3\ mol^{-1}\ cm^{-1}$.[44] The concentration of the compounds was kept constant at 1×10^{-5} M and the concentration of DNA varied from 0 to 100 μM. The binding constants (K_b) were determined using the equation

$$\frac{[DNA]}{\varepsilon_a - \varepsilon_f} = \frac{[DNA]}{\varepsilon_b - \varepsilon_f} + \frac{1}{K_b(\varepsilon_b - \varepsilon_f)}$$

where [DNA] is the concentration of DNA and ε_a, ε_f and ε_b correspond to the apparent extinction coefficient, the extinction coefficient of unbound compound and the extinction coefficient of fully bounded compound, respectively. A plot of $[DNA]/(\varepsilon_a - \varepsilon_f)$ versus [DNA] gives the binding constant K_b as the ratio of the slope to the intercept.[34,45]

DNA binding with **1**–**3** was also measured by a fluorescence spectral technique; EB displacement assay from EB-bound CT-DNA in Tris–HCl buffer at biological pH (7.4) was done. EB was used as it is non-emissive in Tris–HCl buffer solution (pH = 7.4) because of fluorescence quenching of independent EB by the solvent. Absorption titration was carried out by keeping the CT-DNA and EB concentrations fixed at 10 and 20 μM, respectively, while changing the **1**–**3** concentration from 0 to 130 μM. Furthermore, the fluorescence intensity change at 605 nm (520 nm excitation) of EB (20 μM) attached to DNA was measured as a function of the concentration of **1**–**3** (0 to 130 μM).

4.6 | BSA binding studies

The interaction of **1**–**3** with BSA was studied through tryptophan emission quenching experiments. Emission intensity of BSA at $\lambda = 340$ nm. Solutions of **1**–**3** were gradually added to a solution of BSA (5 μM) in 50 μM Tris–HCl buffer (pH = 7.4) and the emission signals which showed quenching were recorded at 340 nm ($\lambda_{ex} = 295$ nm).

4.7 | CD measurements

CD spectroscopy of BSA in the presence of **1**–**3** was conducted using a JASCO 720 spectropolarimeter equipped with a Peltier temperature control device at 298 K under a continuous flow of nitrogen purge. All the experiments were performed in a 1 mm path length quartz cell. Three successive scans were recorded at a scan speed of 50 nm cm^{-1} and their average was considered to obtain the CD spectra of BSA. The results were obtained by the deduction of Tris–HCl (blank). The information of the change in secondary structure of BSA was achieved by far UV–CD spectra (200–260 nm). First, the spectra of free BSA (10 μM) were recorded and then the CD spectral changes were observed by monitoring the binding of BSA while adding 15 and 30 μM of **1**–**3** successively.

4.8 | Synthesis of compound 1

To a stirred solution of 9,10-dibromoanthracene (0.20 mmol) and ethynylferrocene (0.45 mmol) in 40 ml of THF and 40 ml of TEA (1:1, *v*/v), $Pd(PPh_3)_4$ (32 mg, 0.028 mmol) was added under an inert atmosphere at RT. The reaction mixture was stirred for 15 h at 75 °C and monitored by TLC. The reaction solvent was then removed under reduced pressure, the crude mixture was dissolved in DCM, passed through celite and again dried. Further, the separation was carried out by SiO_2 chromatography with DCM–hexane (2:3, v/v) to obtain **1** as a red-coloured solid. Brown red crystals were obtained in DCM–hexane (4:1) in 5 days.

Characterization data. ^{1}H NMR (400 MHz, $CDCl_3$, δ, ppm): 4.37 (s, 10H, C_5H_5), 4.42 (s, 4H, C_5H_4), 4.77 (s, 4H, C_5H_4), 7.64 (4H, non-terminal ant.-H), 8.63 (4H, terminal ant.-H). ^{13}C NMR (100.635 MHz, $CDCl_3$, δ, ppm): 14.2; 22.8; 31.9; 50.8; 68.9; 70.9; 72.4; 80.2; 121.1; 155.5; 191.1. IR (KBr, cm^{-1}): 3091.93, 3060.15, 2957.68, 2201.23, 1620.14, 1412.41, 1390.11, 915.36, 820.06, 762.24, 638.30. $\lambda_{max} = 443$, 513 nm. HRMS (*m*/*z*): [M] calcd for $C_{38}H_{26}Fe_2$, 594.07; found, 594.07.

4.9 | Synthesis of compound 2

To a stirred solution of 1,8-dibromoanthracene (0.20 mmol) and ethynylferrocene (0.45 mmol) in 40 ml of THF and 40 ml of TEA, $Pd(PPh_3)_4$ (40 mg, 0.035 mmol) was added under an inert atmosphere at RT. Further procedure followed as for **1**. Compound **2** was obtained as a red solid. Dark red crystals were obtained in DCM–hexane (4:1) in 5 days.

Characterization data. ^{1}H NMR (400 MHz, $CDCl_3$, δ, ppm): 4.25 (s, 10H, C_5H_5), 4.25 (s, 4H, C_5H_4), 4.63 (s, 4H, C_5H_4), 7.46 (t, $J = 8$ Hz, 2H, pos. 3,6), 7.77 (d, $J = 8$ Hz, 2H, pos. 2,7), 7.99 (d, $J = 8$ Hz, pos. 4,5), 8.45 (s, 1H, pos.10), 9.46 (s, 1H, pos.9). ^{13}C NMR (100.635 MHz, $CDCl_3$, δ, ppm): 65.3; 68.9; 70.1; 71.9 84.2; 94.1; 122.2; 124.2; 125.2; 128; 129.9; 131.6. IR (KBr, cm^{-1}): 3095.05, 3047.58, 2924.17, 2205.48, 1632.20, 1319.20, 1104.03, 1020.30, 880.67, 745.64, 524.60. $\lambda_{max} = 390$, 413 nm. HRMS (*m*/*z*): [M] calcd for $C_{38}H_{26}Fe_2$, 594.07; found, 594.08.

4.10 | Synthesis of compound 3

To a stirred solution of 2,6-diiodoanthraquinone (0.20 mmol) and ethynylferrocene (0.45 mmol) in 40 ml of toluene and 40 ml of TEA (1:1, *v*/v), $Pd(PPh_3)_4$ (40 mg, 0.035 mmol) was added under an inert atmosphere at RT. The reaction mixture was stirred for 15 h at 90 °C. Further procedure followed as for **1**. Compound **3** was obtained as a red-coloured solid. Red crystals were obtained in DCM–hexane (4:1) in 8 days.

Characterization data. ^{1}H NMR (400 MHz, $CDCl_3$, δ, ppm): 4.28 (s, 10H, C_5H_5), 4.33 (s, 4H, C_5H_4), 4.57 (s, 4H, C_5H_4), 7.84 (d, $J = 8$ Hz, 2H, pos. 3,7), 8.27 (d, $J = 8$ Hz, 2H, pos. 4,8), 8.32 (s, pos. 1), 8.37 (s, pos. 5). ^{13}C NMR (100.635 MHz, $CDCl_3$, δ, ppm): 14.2; 24.9; 25.9; 31.5; 62.2; 70.3; 10.7; 113.9; 135.3; 14.4; 153.6. IR (KBr, cm^{-1}): 3103.71, 2924.45, 2853.69, 2204.61, 1672.05, 1591.35, 1413.30, 1312.29, 1281.13, 1106.65, 1035.59, 919.19, 822.83, 743.02, 710.67. $\lambda_{max} = 360$, 515 nm. HRMS (*m*/*z*): [M] calcd for $C_{38}H_{26}Fe_2$, 624.04; found, 624.1.

ACKNOWLEDGEMENTS

We are grateful to the Single Crystal X-ray Diffraction Facility equipped at the Sophisticated Instrumentation Centre (SIC), IIT Indore. S.M.M. acknowledges CSIR, New Delhi and IIT Indore for funding. A.S. thanks UGC, New Delhi for providing a fellowship. P.M. gratefully acknowledges the J. C. Bose National Fellowship.

ORCID

Ajeet Singh http://orcid.org/0000-0002-2665-5123
Shaikh M. Mobin http://orcid.org/0000-0003-1940-3822

REFERENCES

[1] G. Tabbì, C. Cassino, G. Cavigiolio, D. Colangelo, A. Ghiglia, I. Viano, D. Osella, *J. Med. Chem.* **2002**, *45*, 5786.

[2] P. J. Dyson, G. Sava, *Dalton Trans* **2006**, 1929.

[3] B. Zhou, J. Li, B.-J. Feng, Y. Ouyang, Y.-N. Liu, F. Zhou, *J. Inorg. Biochem.* **2012**, *116*, 19.

[4] X. Huang, L. Wang, L. Tang, Y. Lu, F. Wang, G. Song, B. Ruan, *J. Organometal. Chem.* **2014**, *749*, 157.

[5] C. Roux, C. Biot, *Future Med. Chem.* **2012**, *4*, 783.

[6] C. Biot, N. François, L. Maciejewski, J. Brocard, D. Poulain, *Bioorg. Med. Chem. Lett.* **2000**, *10*, 839.

[7] D. Dive, C. Biot, *ChemMedChem* **2008**, *3*, 383.

[8] R. Rubbiani, O. Blacque, G. Gasser, *Dalton Trans.* **2016**, *45*, 6619.

[9] V. N. Babin, Y. A. Belousov, V. I. Borisov, V. V. Gumenyuk, Y. S. Nekrasov, L. A. Ostrovskaya, I. K. Sviridova, N. S. Sergeeva, A. A. Simenel, L. V. Snegur, *Russ. Chem. Bull.* **2014**, *63*, 2405.

[10] M. C. Núñez, M. G. Pavani, M. Díaz-Gavilán, F. Rodríguez-Serrano, J. A. Gómez-Vidal, J. A. Marchal, A. Aránega, M. A. Gallo, A. Espinosa, J. M. Campos, *Tetrahedron* **2006**, *62*, 11724.

[11] S. Pedotti, A. Patti, S. Dedola, A. Barberis, D. Fabbri, M. A. Dettori, P. A. Serra, G. Delogu, *Polyhedron* **2016**, *117*, 80.

[12] C. Ornelas, *New J. Chem.* **2011**, *35*, 1973.

[13] W.-H. Piao, R. Wong, X.-F. Bai, J. Huang, D. I. Campagnolo, R. T. Dorr, T. L. Vollmer, F.-D. Shi, *J. Immunol.* **2007**, *179*, 7415.

[14] P. Lee, X. Wu, *Curr. Pharm. Des.* **2015**, *21*, 1862.

[15] C. L. Freeman, R. Swords, F. J. Giles, *Expert Rev. Hematol.* **2012**, *5*, 17.

[16] S. Kaur, S. Dhoun, G. Depotter, P. Kaur, K. Clays, K. Singh, *RSC Adv.* **2015**, *5*, 84643.

[17] R. D. A. Hudson, I. Asselberghs, K. Clays, L. P. Cuffe, J. F. Gallagher, A. R. Manning, A. Persoons, K. Wostyn, *J. Organometal. Chem.* **2001**, *637–639*, 435.

[18] N. Chawdhury, N. J. Long, M. F. Mahon, L. Ooi, P. R. Raithby, S. Rooke, A. J. P. White, D. J. Williams, M. Younus, *J. Organometal. Chem.* **2004**, *689*, 840.

[19] A. Caballero, R. Tormos, A. Espinosa, M. D. Velasco, A. Tárraga, M. A. Miranda, P. Molina, *Org. Lett.* **2004**, *6*, 4599.

[20] V. Mishra, A. Raghuvanshi, A. K. Saini, S. M. Mobin, *J. Organometal. Chem.* **2016**, *813*, 103.

[21] A. K. Saini, P. Kumari, V. Sharma, P. Mathur, S. M. Mobin, *Dalton Trans.* **2016**, *45*, 19096.

[22] A. Robertazzi, A. V. Vargiu, A. Magistrato, P. Ruggerone, P. Carloni, P. de Hoog, J. Reedijk, *J. Phys. Chem. B* **2009**, *113*, 10881.

[23] Y.-H. Ding, Z.-W. Zhou, C.-F. Ha, X.-Y. Zhang, S.-T. Pan, Z.-X. He, J. L. Edelman, D. Wang, Y.-X. Yang, X. Zhang, W. Duan, T. Yang, J.-X. Qiu, S.-F. Zhou, *Drug Des. Devel. Ther.* **2015**, *9*, 425.

[24] L.-W. Zheng, L.-L. Wu, B.-X. Zhao, W.-L. Dong, J.-Y. Miao, *Bioorg. Med. Chem.* **2009**, *17*, 1957.

[25] G. Jaouen, A. Vessières, S. Top, *Chem. Soc. Rev.* **2015**, *44*, 8802.

[26] J. R. Lakowicz, *Principles of Fluorescence Spectroscopy*, Springer, Boston, MA **2006**.

[27] V. D. Suryawanshi, L. S. Walekar, A. H. Gore, P. V. Anbhule, G. B. Kolekar, *J. Pharm. Anal.* **2016**, *6*, 56.

[28] Z. Cheng, R. Liu, X. Jiang, *Spectrochim. Acta A* **2013**, *115*, 92.

[29] M. van de Weert, L. Stella, *J. Mol. Struct.* **2011**, *998*, 144.

[30] A. Ray, B. Koley Seth, U. Pal, S. Basu, *Spectrochim. Acta A* **2012**, *92*, 164.

[31] I. M. Kuznetsova, A. I. Sulatskaya, O. I. Povarova, K. K. Turoverov, *PLoS One* **2012**, *7*, e40845.

[32] E.-H. Liu, L.-W. Qi, P. Li, *Molecules* **2010**, *15*, 9092.

[33] M. Möller, A. Denicola, *Biochem. Mol. Biol. Educ.* **2002**, *30*, 309.

[34] A. Patra, S. K. Saha, T. K. Sen, L. Carrella, G. T. Musie, A. R. Khuda-Bukhsh, M. Bera, *Eur. J. Inorg. Chem.* **2014**, 5217.

[35] M. Das, R. Nasani, M. Saha, S. M. Mobin, S. Mukhopadhyay, *Dalton Trans.* **2015**, *44*, 2299.

[36] J. G. Lees, A. J. Miles, F. Wien, B. A. Wallace, *Bioinformatics* **2006**, *22*, 1955.

[37] N. J. Greenfield, *Nat. Protoc.* **2007**, *1*, 2876.

[38] G. M. Sheldrick, *Acta Crystallogr C* **2015**, *71*, 3.

[39] M. Frisch, G. Trucks, H. Schlegel, G. Scuseria, M. Robb, J. Cheeseman, G. Scalmani, V. Barone, B. Mennucci, G. Petersson, et al., *Gaussian 09, Revision A.02*, Gaussian Inc., Wallingford, CT **2009**.

[40] A. D. Becke, *J. Chem. Phys.* **1993**, *98*, 5648.

[41] C. Lee, W. Yang, R. G. Parr, *Phys. Rev. B* **1988**, *37*, 785.

[42] G. M. Morris, D. S. Goodsell, R. S. Halliday, R. Huey, W. E. Hart, R. K. Belew, A. J. Olson, *J. Comput. Chem.* **1998**, *19*, 1639.

[43] N. Patel, P. V. Oudemans, B. I. Hillman, D. Y. Kobayashi, *Antonie Van Leeuwenhoek* **2013**, *103*, 1271.

[44] S. Bhattacharyya, A. Sarkar, S. K. Dey, G. P. Jose, A. Mukherjee, T. K. Sengupta, *Dalton Trans.* **2013**, *42*, 11709.

[45] E. Sundaravadivel, S. Vedavalli, M. Kandaswamy, B. Varghese, P. Madankumar, K. Natarajan, P. Cheng, Z. Guo, C. Santos, *RSC Adv.* **2014**, *4*, 40763.

SUPPORTING INFORMATION

Additional Supporting Information may be found online in the supporting information tab for this article.

How to cite this article: Singh A, Kumari P, Raghuvanshi A, Mobin SM, Mathur P. Ferrocene-substituted bis(ethynyl)anthracene compounds as anticancer agents. *Appl Organometal Chem*. 2017; e4071. https://doi.org/10.1002/aoc.4071